INTERLAMINAR FRACTURE OF COMMINGLED GF/PET COMPOSITE LAMINATES

Niklas Svensson

Pelmatic Consulting Engineers, F O Petersons gata 28, SE42131 Västra Frölunda, SWEDEN

Phone: +46-31-709 31 00, E-mail: niklas.svensson@pelmatic.com

Roshan Shishoo

Swedish Institute for Fiber and Polymer Research, P.O.Box 104, SE43122 Mölndal, SWEDEN

Phone: +46-31-706 63 00, E-mail: roshan.shishoo@ifp.se

Michael Gilchrist*

Department of Mechanical Engineering, University College Dublin, Belfield, Dublin 4, IRELAND

Phone: +353-1-706 18 90, E-mail: Michael.Gilchrist@ucd.ie

* corresponding author

ABSTRACT

The Mode I, Mode II and mixed mode (Mode I:II ratios of 4:1, 1:1 and 1:4) fracture behavior of novel textile glass fiber reinforced polyethylene terephthalate (GF/PET) laminates has been investigated. The laminates were manufactured by compression molding two different fabrics produced by weaving and warp knitting commingled GF/PET yarns. The initiation fracture toughnesses of the woven laminates in pure Mode I and Mode II were slightly higher than those of the warp knitted laminates. For the mixed modes, the difference between the fracture toughnesses of the two materials was smaller. An extensive scanning electron microscopy (SEM) investigation of the fracture surfaces was conducted to identify any characteristic failure mechanisms. The main fractographic features of the Mode I dominated failures were a brittle matrix failure and large amounts of fiber pull-out. As the Mode II loading component increased, the amount of fiber pull-out was reduced and the matrix had a more sheared appearance. A relatively large amount of cusps were found in pure Mode II and mixed mode I:II=1:4; such features are seldom seen in thermoplastic matrix composites. A general mixed mode failure criterion, which accounts for the appearance of the fracture surface, was evaluated and was seen to give a good fit to the experimental fracture toughness values.

KEYWORDS: commingled yarn, cusps, fractography, mixed mode bending, mixed mode failure criterion, interlaminar fracture

INTRODUCTION

Fracture mechanics approaches are commonly used for modeling delamination growth in composite structures. The resistance to interlaminar crack growth is expressed by the material fracture toughness, which is defined as the energy required to propagate a crack from an inherent

defect. Crack propagation can occur in a combination of three modes: tensile opening or Mode I, sliding shear or Mode II, and tearing shear or Mode III, as shown schematically in Figure 1. The fracture toughnesses in the respective modes are denoted G_{IC}, G_{IIC} and G_{IIIC}.

Failures in pure Mode I or pure Mode II are rare and, consequently, methods for determining the mixed mode fracture properties of composites are important. The mixed mode bending (MMB) jig developed by Crews and Reeder [2] enables a variety of mixed modes to be examined using a simple beam specimen and this method has been used widely in recent years [3-7]. The same specimen dimensions are used for all mixed modes and inconsistencies due to specimen configurations are avoided [4]. Reeder and Crews [3] later proposed modifications to the MMB test to minimize the geometric non-linearity and the non-linearity errors were reduced to less than 3% even for tough materials such as APC2. Kinloch et al. [5] studied the MMB test in detail and proposed correction factors for large deformations. Partitioning the interlaminar fracture energy is best carried out by a global method based upon a consideration of the applied energy release rates where Mode I is pure tension and Mode II is pure shear [5,8].

To improve the fracture performance in composites a tough thermoplastic matrix may be used. However, an increased matrix toughness does not necessarily lead to a large increase in the laminate toughness and three reasons for this are [9]; (i) premature failure may occur due to a weak fiber/matrix interface, (ii) the fibers provide a constraint which changes the stress state and limits the ductility of the resin, and (iii) the fibers act as rigid fillers and reduce the volume of material available for deformation. Friedrich [10] suggested the following principle micro mechanisms for energy absorption; crack bridging by fibers or fiber bundles; fiber breakage from the bridging; formation of the fracture surface features; formation of secondary cracks outside the main crack and plastic deformation and/or micro cracking of matrix around fibers. The maximum toughness is achieved when no low energy fiber/matrix interfacial debonding is present [11].

Commingled yarns are promising material systems for producing thermoplastic composites. The yarns contain both spun matrix fibers and reinforcing fibers which are intimately mixed at

the filament level. Dry preforms can hence be easily produced using a variety of techniques, e.g. weaving, braiding and knitting. Application of heat and pressure is required for the consolidation in which the thermoplastic fibers melt and impregnate the reinforcing fibers. Due to the close intermingling of the reinforcing fibers and the matrix fibers the required matrix flow distance is very small. The manufacturing and mechanical properties of commingled thermoplastic composites have been studied extensively by Svensson et al. [12,13]. Previous work on interlaminar fracture of commingled thermoplastic composites has focused on unidirectional laminates, either carbon fiber/poly ether ether ketone composites (CF/PEEK) [14-17] or glass fiber/polypropylene composites (GF/PP) [18-20], in Mode I and/or Mode II. However, Ye and Friedrich [21] determined the Mode I and Mode II fracture toughnesses of woven biaxial commingled glass fiber/polyethylene terephthalate (GF/PET) laminates. The PET matrix was seen to be almost insensitive to changes in the thermal history compared to polypropylene (PP). This was also supported by Shonaike et al. [22]. Table 1 summarises the fracture toughness values available in literature for a number of commingled composites.

The present work is concerned with the Mode I, Mode II and mixed mode characteristics of textile commingled GF/PET laminates. Two different novel fabrics were used for the manufacturing of laminates. The characteristic fracture features are identified and the suitability of using a mixed mode failure criterion to predict the performance of these composite materials is discussed.

EXPERIMENTAL

The fabrics were produced from commingled E-glass fibers/PET yarns by means of warp knitting and weaving, Figure 2. The yarns were used as received from the supplier and no information on the glass fiber surface treatment was available to the present authors. The woven fabrics had the main fraction (5/6) of the yarns in the warp direction while the warp knitted fabric was unidirectional and the commingled warp yarns were held together with a thin PET binding yarn. The fabrics were cut and stacked in the appropriate number of layers to produce unidirectional laminates. 20 layers were used for the warp knitted fabric and 12 for the woven fabric. The fabrics were kept at room temperature prior to the compression molding. Spacers were used to obtain a uniform laminate thickness of 3mm. The consolidation pressure was hence provided by the compaction of the fabric stack from the uncompressed thickness of about 12mm to 3mm.

The laminates were compression molded in a hydraulic press between steel platens which had been previously coated with release agent. The mold was heated to 220ºC within 20min and was held at that temperature for 20min. Circulating water was used for cooling the mold and the cooling rate was about 21°C/min. A 50μm thick Nylon6 film, coated with a poly tetra fluoro ethylene (PTFE) release agent, was used to induce the starter cracks in the laminates.

The T_g of the PET matrix was determined to be 75.8°C. After the compression molding some of the woven laminates were annealed for three hours at 110ºC to promote spherulite growth. The reason for this was to investigate if any differences in mechanical properties could be observed as a result of the different thermal histories of the laminates.

The mechanical properties of the two materials in tension, flexure and shear were determined [12] and are summarized in Table 2.

The fracture specimens were cut using a band saw and the edges of the specimens were polished and coated with typewriter correction fluid and the crack tip was marked along the edges of the specimens. The specimen dimensions were as prescribed by the ASTM D5528 standard for

Mode I characterization of unidirectional composite materials using the DCB (Double Cantilever Beam) method.

The Mode I characterization was carried out using the DCB test method. For pure Mode II and the mixed mode I:I = 4:1, 1:1 and 1:4 tests (Mode I to Mode II loading ratio) the modified MMB jig was used, Figure 3. A minimum of four specimens were tested for each mode and material.

RESULTS AND DISCUSSION

The fabrics were tailored and manufactured to be unidirectional, in the case of the warp knitted fabric, and mainly unidirectional, for the woven. A characterization of the formability of the fabrics using the Kawabata Evaluation System showed that these fiber architectures gave a very high flexibility in the weft direction. This made the fabrics relatively difficult to handle and align during stacking and some variation in fiber angles and fiber volumes was expected in and between the laminates. Distortion of the fiber architecture may also have occurred due to the contraction of the thermoplastic fibers on heating. A further possible reason for the fiber misalignment may be the stiffness mismatch of the polymer and glass filaments causing these to get separated when tension is applied in processes such as filament winding or weaving [20].

The quality of the laminates was examined using optical microscopy of polished cross-sections and generally few voids were seen. Matrix rich pockets appeared and these originated from the fiber architecture that had been used. The number of matrix pockets was higher in the woven laminates than in the warp knitted laminates and the matrix pockets were formed where the warp and weft yarns met. An optical micrograph from a woven laminate is seen in Figure 4. The crimp in the fiber architecture is seen as well as a number of matrix pockets. Outside the pockets the fiber distribution is good. Occasionally, cracks were seen in and between the fiber bundles; these were also observed by Ye and Friedrich [21].

The adhesion between the glass fibers and the PET matrix was seen to be poor which might be due to the fact that the processing parameters for this particular material system has not yet been

optimized. Reports on the interfacial quality in GF/PET composites in previous work vary between good and poor. Figure 5 shows a glass fiber that has been pulled out from the matrix which has been deformed substantially during the pull-out process.

Mode I

The Mode I tests were carried out using the DCB test. Unstable crack growth was observed in about half of the specimens, as can be seen in the non-monotonic reduction in load after initial crack growth in Figure 6. No difference was seen between the fracture behavior of the woven and the warp knitted laminates and the load/displacement curves were non-linear before the maximum load was reached. During the tests a large amount of fiber pull-out was seen, Figure 7, and this contributed to the high apparent fracture toughness and the unstable crack growth. The initiation value of the fracture toughness was calculated at the point where the load/deflection curve deviated from linearity. The propagation values were calculated at the steady state crack growth. Table 3 shows the initiation and propagation fracture toughness values for the three different materials. No difference was seen between the annealed woven laminate and the ordinary woven laminate. The fracture toughness of the warp knitted laminates was only slightly lower than for the woven laminates and this may be due to the weft yarns which effectively prevented crack propagation in the woven laminates. This agrees well with the work of Yoon and Takahashi [14] on Mode I interlaminar fracture of CF/PEEK composites who reported that the cracks were arrested by the weft yarns and that a higher stress was needed to reinitiate the cracks. The higher stress resulted in higher crack propagation rates and faster and more unstable crack growth.

A fractographic examination of the Mode I fracture specimens showed that the most dominant surface characteristic was fiber pull-out. The global crack propagation direction in all SEM micrographs (Figures 8-23) is from the bottom to the top. Figure 8 shows a large amount of fiber pull-out at the end of the non-adhesive insert in a warp knitted specimen. Some of the pulled out

fibers extended back into the insert area and this might have contributed to the high resistance to crack initiation. The amount of fiber pull-out was larger for the warp knitted laminates. The pull-out mainly occurred in bundles and this was also observed previously in similar work on multidirectional carbon fiber/epoxy laminates [23]. In the woven laminates, the weft yarns prevented extensive pull-out of the fibers and yarns in the warp direction. The poor strength of the fiber/matrix interface promoted fiber pull-out. The amount of fiber ends on the fracture surface in multidirectional T300/914 was investigated for Mode I, Mode II and a number of mixed modes by Svensson and Gilchrist [7]. Friedrich [10] had previously shown this feature to be significantly different for Mode I and Mode II. However, this characteristic was seen to be of only marginal importance in the material systems of the present work. The general trend that was observed was that the fiber end density decreases rapidly from pure Mode I to Mode II dominated modes. As the amount of fiber pull-out is dependent on specimen and material parameters [10,24] this method cannot be used reliably to characterize different fracture modes. In testing woven CF/PEEK laminates, Beehag and Ye [15], observed that the amount of fiber bridging was not consistent between the tests.

The matrix failed in a brittle manner as seen in Figure 9. Figure 10 shows the general Mode I surface appearance of woven laminates with a featureless brittle matrix failure and imprints from pulled out fibers. The warp and weft yarns are also seen and these were not always perpendicular to each other due to the misalignment discussed earlier. No spherulites could be seen in any of the specimens and no microstructural difference could be detected between the two woven materials. The misalignment of fibers in commingled laminates causes extensive fiber bridging during crack propagation, both in Mode I and Mode II.

Ye and Friedrich [20] studied the Mode I fracture behavior of UD GF/PP laminates. They reported interspherulitic fracture paths between the debonded areas and a toughness that was much lower in slowly cooled laminates with large voids and coarse spherulites than for the rapidly cooled specimens. Resin rich areas existed between the glass fiber bundles in which the

fiber volume fraction was very high. Large amounts of fiber bridging and breakage behind the crack tip were seen and the fiber bridges were continuously formed and broken. Sub-critical crack branching was observed in front of the main cracks. Many bundles remained intact and peeled over the full length of the test specimen. This led the authors to the development of a model for the total Mode I fracture energy of commingled laminates [20] which showed that the contributions to Mode I fracture energy from fiber peeling and breakage were much larger than those from matrix deformation.

The Mode I crack propagation of woven GF/PET laminates was a combination of stable and unstable crack growth [21]. Clear non-linearities were observed in the load/displacement curve before reaching the maximum load. Only small amounts of fiber pull-out were seen as the weft bundles prevented further pull-out. The fibers were disturbed during the compression molding by the matrix flow, which resulted in non-unique delamination planes with crack growth in resin rich regions and fiber bundle borders. Crack branching was observed in front of the main crack tip at the intersection of weft bundles; this lead to an increase in the apparent interlaminar fracture toughness.

Mode II

Crack propagation during the Mode II fracture tests was more stable than during the Mode I tests, even for the woven materials, Figure 11. The crack initiation values were calculated at the onset of non-linearity of the load/displacement curve and the propagation energy was calculated as an average of the stable crack growth fracture toughness values. The warp knitted laminates had a fracture toughness that was only marginally lower than that of the woven laminates, both in initiation and propagation, Table 4.

The most important fractographic matrix feature is cusps which, in the literature, also have been referred to as hackles, lacerations, scallops, platelets, shingles, a stacked lamellar structure and serrations. Purslow [25] rightfully recognized the need to develop a general terminology. It is

generally accepted that the matrix in the interlaminar region ahead of the crack tip will crack in a brittle manner due to the resolved stresses to which it is subjected. When a Mode II component of load is present, crack propagation in a brittle matrix occurs by the coalescence of sigmodial shaped microcracks as observed [9,11] by means of in-situ scanning electron microscopy (SEM). The coalescence occurs near the fiber/matrix interface at the upper or lower boundary of the interlaminar region. When coalescence has started at one ply interface it will continue there as the stress redistribution involved will favor a continued coalescence at the same interface [9].

In pure Mode II loading the cracks would, according to the maximum principal stresses, form at an angle of 45° to the fracture plane. This angle would decrease with an increasing amount of Mode I loading and for pure Mode I no cusps would form [26]. Experimental evidence supports this qualitatively [6,26-28] and lately also quantitatively [7]. Cusp angles significantly greater than 45° have been observed. An explanation for this was suggested by Hibbs and Bradley [9]; the cusps attain a more inclined position as a result of cusp rotation due to shear loading just prior to the microcrack coalescence. This rotation would position the microcrack more vertically and open up the microcrack where the coalescence takes place. Also, the cusp angles appear to be independent of the actual material system which supports the theory for microcrack formation.

Cusps are only found in relatively brittle systems as they are formed from microcrack nucleation ahead of the crack tip [9]. Due to their higher ductility the number of cusps decreases in tougher resins, which is the reason for their lower ratio of G_{IIC}/G_{IC} [29]. Reeder [4] observed that cusps appeared in epoxy matrices at mixed modes 1:1 and other mixed modes with a larger Mode II component. In PEEK laminates no cusps were seen at any loading mode. Observations of cusp formation in thermoplastic matrix composites has, however, been very scarce. Ye and Friedrich [21] reported the formation of slanted cracks on the edge of commingled GF/PET specimens during Mode II testing but did not refer to them as cusps.

In the present work, for both the woven and warp knitted laminates, a relatively large amount of cusps was observed on the Mode II fracture surfaces, as can be seen from Figures 12-14. The

formation of cusps has been attributed to a brittle failure of the matrix and this indicates that the PET matrix in this composite failed in a fairly brittle manner. This was also supported by the appearance of the matrix failure in Mode I fracture (Figure 9). Shear deformation of the matrix was also seen, Figure 15, but this was not as extensive as in previous work on other thermoplastic matrix composites such as CF/PEEK [17]. It is possible that hydrolysis may account for some of the brittleness seen in the matrix. Due to the relatively thick inserts that were used, large matrix pockets were seen at the end of the inserts, typically as shown in Figure 16, and these might also have increased the initiation fracture toughness of the laminates. Figure 17 shows a micrograph of the crack front in a warp knitted Mode II fracture specimen at low magnification. At the bottom of the micrograph, the fracture is seen to have propagated in Mode II and the top half shows a typical Mode I fracture surface where the specimen was broken up manually. The Mode II fracture is more matrix dominated and has less fiber pull-out.

Wavy lamina were formed in the woven CF/PEEK laminates [15] because of the fabric architecture which lead to an uneven and irregular interlaminar fracture path. This, in turn, gave a high apparent fracture toughness. Matrix rich regions ahead of the simulated delamination (non-adhesive film insert) and a wavy starter delamination may also occur due to the structure of the carbon fibers. In the woven laminates of the present work the cracks were seen to follow the undulation of the warp yarns during propagation.

In the woven GF/PET laminates examined by Ye and Friedrich [21], the Mode II propagation was generally unstable. The crack initiation took place at a small kink at an angle of 30-65°. As the load increased, more cracks developed and extended and these resulted in a non-linearity in the load/displacement curve. Coalescence of the cracks occurred after maximum loading. Increases in the level of crystallinity lead to reductions in both the Mode I and Mode II crack propagation energies. The SEM observations identified characteristic brittle failures on all fracture surfaces. A large amount of small voids, of the same dimensional order as the fibers, were seen in the resin rich regions. The glass fibers were always coated with resin, which was

indicative of a good interfacial bond. No evidence of interspherulitic fracture paths could be seen. The matrix that had been quenched was able to sustain much more deformation than that which was produced under slow cooling. The authors concluded that it is important to avoid slow cooling in order to prevent the formation of spherulites, microcracks and voids all of which contribute to a large decrease in crack propagation energies in both Modes I and II.

Mixed modes

Some problems were encountered in the mixed mode fracture tests using the MMB jig. The large deflections that were present due to the tough matrix and the low modulus glass fibers resulted in the loading lever sometimes contacting either the end of the specimen or the base of the jig and consequently these tests finished before ultimate fracture of the specimens. This lead to a reduction in the amount of available data for calculating steady state crack propagation energies. The jig has since been modified to handle these large deflections. Stable mixed mode crack growth was seen in most cases for both the warp knitted and the woven laminates. The crack initiation and propagation energies for the three materials in the three different mixed modes are given in Table 5. The mixed mode I:II = 4:1 fracture surfaces had an appearance similar to the Mode I fracture surfaces with fiber pull-out and brittle, featureless matrix failure. Figure 18 shows the area around the insert in a woven specimen tested at mixed mode I:II = 4:1. In the micrograph it is seen that the insert in this particular laminate ended in a weft bundle (running from left to right in the micrograph) and this may have affected the crack initiation. The matrix is featureless and there are plenty of imprints from pulled-out fibers. In Figure 19 a large fractured matrix pocket in a woven laminate can be seen. The mode of fracture in this case was I:II = 1:1. The matrix has a rougher appearance in this mode than in the I:II = 4:1 mode. Very clean fibers are seen. The previously discussed local misalignment of fibers that occurred during manufacturing is evident in Figure 20, which shows the fracture surface of a woven mixed mode I:II = 1:1 sample at low magnification.

Cusps were also found in the Mode II dominated mixed modes, Figures 21 and 22. However, the amount of cusps was much smaller than for pure Mode II. Compared to brittle epoxy matrix composites, cusps in this material system are very rare and are not as well defined, i.e. the cusps vary in size and appearance (compare Figures 13, 14 and 22). The cusps also seemed to stand more upright than the cusps previously observed in epoxy matrices [7]. Evidence for the

previously discussed proposed theory of cusp formation was also found. A number of slanted microcracks, just prior to coalescence, are seen in Figure 23.

Failure criterion

A general mixed mode criterion, including a parameter, ω, called the slope of the fracture surface roughness, was proposed by Charalambides et al. [8]. This is shown in Eq. (1) where G_C is the total measured fracture energy, G_0 is the induced Mode I component of fracture energy, ψ the phase angle of the applied loads, ψ_0 is the phase angle due to the elastic mismatch across a bimaterial interface and ω is the slope of the fracture surface roughness. The surface roughness, ω, which is 0° for smooth fracture surfaces, is material and fracture process dependent [8] and, in the criterion, this is calculated directly from the experimentally determined Mode I and Mode II fracture toughnesses.

$$G_0 = G_c\left(\cos^2\left(\psi - \psi_0\right) + \sin^2\omega\sin^2\left(\psi - \psi_0\right)\right) \qquad (1)$$

A modification to one of the parameters of this criterion was proposed by Svensson and Gilchrist [7]. By assuming that the ω-parameter is the actual cusp angle as measured physically instead of predicted analytically and by using experimentally determined measures of the cusp angles, the failure locus changed. The modified criterion gave a peak at a mixed mode ratio of approximately I:II = 1:1, which agreed well with observations by Reeder [4] who reported that fracture toughness data of epoxy composites reach a peak at this ratio. The fit to experimental fracture toughness data of T300/914 carbon fiber/epoxy was better for the modified criterion than for the original criterion. This is discussed below in greater detail for the present material system.

The failure criterion proposed by Charalambides et al. [8] was evaluated for the three different materials. As can be seen from the graphs in Figure 24, the criterion generally gave a good fit.

However, for the warp knitted laminates the mixed mode fracture toughness values were relatively higher than the values for pure Mode I and Mode II. This was not predicted by the criterion. The reasons for the high mixed mode values are not fully understood.

ω, Charalambides' [8] parameter that represented the slope of the surface roughness, was calculated to be 46.5° for initiation and 45.0° for propagation. The propagation value corresponded very well to the theoretically predicted cusp angles for pure Mode II. For the previously discussed carbon fiber/epoxy system, the value was 52.9°, which was very close to the experimentally determined mode II cusp angle (54.0°) [7]. Charalambides et al. [8] suggested that the surface roughness may well reflect the slope of microcracks formed ahead of the crack front, i.e., the cusp angle. Kinloch et al. [5] determined ω to be 41° for a carbon fiber/epoxy composite, 50° for a carbon fiber/PEEK composite at initiation and 41° for propagation. In the Charalambides et al. [8] study, ω-values of 44° and 46° were seen for the epoxy and PEEK systems, respectively.

Modifications similar to those suggested by Svensson and Gilchrist [7] were made, i.e. the fracture surface roughness parameter was assumed to correspond to the actual cusp angle. Due to the relatively small number of cusps that were present, the cusp angle for each loading mode was not determined experimentally for the laminates in this work and consequently the possibility of using the same cusp angles that had been measured previously by the authors [7] on multidirectional carbon fiber/epoxy was considered. If the formation of cusps is assumed to be due to brittle matrix cracks, similar cusp angles should be observed irrespective of the actual fiber/matrix combination that is used. The results of modifying Charalambides' [8] criterion in this fashion (i.e., by using the values for experimental cusp angles instead of the value of ω predicted analytically by the criterion) for the woven annealed material can be found in Figure 25. The fit is fairly good but the modified criterion overestimates the pure Mode I initiation values and underestimates the Mode II initiation and propagation values. This modified criterion gives a peak around mixed mode 1:1 which previously had been observed by Svensson and

Gilchrist [7] and Reeder [4]. The correspondence between Charalambides' [8] unmodified criterion and the experimentally determined toughnesses is better than that of the modified criterion and consequently it must be concluded that the assumptions associated with this modification are not uniformly valid for all stacking sequences and materials. Variations in cusp angles and the appearance of cusps and of the fracture surface obviously occur between different material systems with different stacking sequences.

Well established fractographic methods for brittle thermoset materials and PEEK composites [10,13,30] may have to be modified when applied to the fracture surfaces of commingled composites because of the absence of a single fracture plane and the very extensive fiber bridging.

CONCLUSIONS

The Mode I, Mode II and mixed mode fracture behavior of glass fiber reinforced poly ethylene terephthalate (GF/PET) laminates was investigated. The laminates were manufactured by compression molding two different fabrics produced by weaving and warp knitting commingled GF/PET yarns. The initiation fracture toughness of the woven laminates in pure Mode I and Mode II failures were slightly higher than for the warp knitted laminates. For the different mixed modes, the difference between the two materials was smaller. Both the crack initiation and crack propagation energies were very high when compared to traditional thermoset matrix composites. The high fracture toughness can be attributed partly to processes such as extensive fiber pull-out caused by a poor fiber/matrix interface and fiber misalignment, the presence of large resin pockets and, in Mode II dominated failures, the deformation of the matrix and the formation of cusps.

A scanning electron microscopy (SEM) investigation of the fracture surfaces was conducted. The main fractographic features of the Mode I dominated failures were a brittle matrix failure and large amounts of fiber pull-out. As the Mode II component of load increased, the amount of fiber

pull-out was reduced and the matrix had a more sheared appearance. A fairly large amount of cusps was found in pure Mode II and in mixed mode I:II=1:4. The present authors are not aware of any reports of cusps in thermoplastic matrix composites.

The failure criterion for mixed mode fracture suggested by Charalambides et al. [8] which accounts for the fracture surface appearance, was evaluated. This was seen to give a very good agreement with the experimentally determined fracture energies except for the mixed mode fracture range in the warp knitted laminates. Modifications to the criterion with previously determined experimental measures of cusp angles for a different material system did not improve the fit for this particular material.

REFERENCES

1. Carlsson, L. A. and Gillespie, J. W., <u>Application of Fracture Mechanisms to Composite Materials</u> Elsevier Science Publishers, Amsterdam, (1989).
2. Crews, J. H. and Reeder, J. R., <u>NASA TM100662</u> (1988).
3. Reeder, J. R. and Crews, J. H., <u>NASA TM102777</u> (1991).
4. Reeder, J. R., <u>NASA TM104210</u> (1992).
5. Kinloch, A. J., Wang, Y., Williams, J. G. and Yayla, P., 1993, <u>Composites Science and Technology,</u> 47:225-237 (1993).
6. Benzeggagh, M. L. and Kenane, M., <u>Composites Science and Technology,</u> 56:439-449 (1996).
7. Svensson, N. and Gilchrist, M., submitted to <u>Mechanics of Composite Materials and Structures</u> (1997).
8. Charalambides, M., Kinloch, A. J., Wang, Y. and Williams, J. G., <u>International Journal of Fracture,</u> 54:269-291 (1992).
9. Hibbs, M. F. and Bradley, W. L., <u>Fractography of Modern Engineering Materials: Composites and Metals, ASTM STP 948</u> American Society for Testing and Materials, (1987).
10. Friedrich, K., <u>Application of Fracture Mechanics to Composite Materials,</u> Elsevier Science Publishers, Amsterdam, (1989).
11. Bradley, W. L., <u>Application of Fracture Mechanics to Composite Materials,</u> Elsevier Science Publishers, Amsterdam, (1989).
12. Svensson, N., Shishoo, R. and Gilchrist, M., <u>accepted for publication in Polymer Composites,</u> (1997).
13. Svensson, N., Shishoo, R. and Gilchrist, M., <u>accepted for publication in Journal of Thermoplastic Composite Materials,</u> (1997).
14. Yoon, H. and Takahashi, K., <u>Journal of Materials Science,</u> 28:1849-1855 (1993).
15. Beehag, A. and Ye, L., <u>Composites Part A,</u> 27A:175-182 (1996).
16. Beehag, A. and Ye, L., <u>Applied Composites Materials,</u> 2:135-151 (1995).
17. Beehag, A. and Ye, L., <u>Journal of Thermoplastic Composite Materials,</u> 9:129-150 (1996).
18. Ye, L., Friedrich, K. and Kästel, J., <u>Applied Composite Materials,</u> 1:415-429 (1995).
19. Ye, L. and Friedrich, K., <u>Journal of Materials Science,</u> 28:773-780 (1993).
20. Ye, L. and Friedrich, K., <u>Composites Science and Technology,</u> 46:187-198 (1993).
21. Ye, L. and Friedrich, K., <u>Composites,</u> 24:557-564 (1993).
22. Shonaike, G. O., Matsuda, M., Hamada, H., Maekawa, Z. and Matsuo, T., <u>Composite Interfaces,</u> 2:157-170 (1994).
23. Gilchrist, M. D. and Svensson, N., 1995, <u>Composites Science and Technology,</u> 55:195-207 (1995).
24. Hu, X. Z. and Mai, Y. W., <u>Composites Science and Technology,</u> 46:147-156 (1993).
25. Purslow, D., <u>Royal Aircraft Establishment, Technical Report 86046</u> (1986).
26. Johannesson, T., Sjöblom, P. and Seldén, R., <u>Journal of Materials Science,</u> 19:1171-1177 (1984).
27. Johannesson, T. and Blikstad, M., <u>Delamination and Debonding of Materials, ASTM STP 876,</u> American Society for Testing and Materials, (1985).
28. Arcan, L., Arcan, M. and Daniel, I. M., <u>Fractography of Modern Engineering Materials: Composites and Metals, ASTM STP 948,</u> American Society for Testing and Materials, (1987).
29. Russell, A. J. and Street, K. N., <u>Toughened Composites, ASTM STP 937,</u> American Society for Testing and Materials, (1987).
30. Purslow, D., <u>Royal Aircraft Establishment, Technical Report 81127</u> (1981).

TABLES

Table 1. The Mode I and Mode II fracture toughness values for commingled composites determined in previous work. The materials are unidirectional and commingled unless otherwise stated.

Material	G_{IC} initiation (kJ/m^2)	G_{IC} propagation (kJ/m^2)	G_{IIC} initiation (kJ/m^2)	G_{IIC} propagation (kJ/m^2)	Ref.
CF/PEEK, prepreg (APC2)	-	1.56	-	-	[14]
CF/PEEK, unidirectional	-	1.98	-	-	[14]
CF/PEEK, woven	-	2.67	-	-	[14]
CF/PEEK, 415°C, 10min consol.	-	-	-	3.0	[15]
CF/PEEK, 415°C, 60min consol.	-	-	-	2.0	[15]
CF/PEEK, rapid cooling	-	3.0	-	2.5	[16]
CF/PEEK, slow cooling	-	1.4	-	1.6	[16]
CF/PEEK, cooling pressure 0MPa	-	1.4	-	1.5	[17]
CF/PEEK, cooling pressure 1.0MPa	-	2.2	-	3.2	[17]
GF/PET, quenched	0.31	0.98	1.34	4.2	[21]
GF/PET, isothermally cryst.	0.17	0.21	0.30	0.73	[21]
GF/PP, quenched	1.0	3.3	-	-	[18]
GF/PP, isothermally cryst.	0.3	1.75	-	-	[18]
GF/PP, small spherulites	0.96	3.29	0.30	4.38	[19,20]
GF/PP, large spherulites	0.17	1.49	0.20	2.20	[19,20]

Table 2. The mechanical properties of the two different GF/PET laminates [12].

	Woven	Warp knitted
Tensile modulus, warp, (GPa)	22.9	28.2
Tensile strength, warp, (MPa)	510.4	486.6
Tensile modulus, weft, (GPa)	6.9	3.5
Tensile strength, weft, (MPa)	130.9	6.6
In-plane shear modulus (GPa)	4.4	4.3
In-plane shear strength (MPa)	98.7	88.4
Flexural modulus, warp, (GPa)	29.0	35.0
Flexural strength, warp, (MPa)	493.6	747.2
Flexural modulus, weft, (GPa)	10.7	4.6
Flexural strength, weft, (MPa)	214.0	24.7

Table 3. The Mode I fracture toughness values determined experimentally for the different laminates and loading modes. The 90% confidence limit is given in brackets.

Material	G_{IC} initiation (kJ/m^2)	G_{IC} propagation (kJ/m^2)
Warp knitted	0.89 (±0.12)	1.14 (±0.06)
Woven	1.13 (±0.09)	1.34 (±0.09)
Woven, annealed	1.15 (±0.20)	1.40 (±0.20)

Table 4. The Mode II fracture toughness values determined experimentally for the different laminates and loading modes. The 90% confidence limit is given in brackets.

Material	G_{IIC} initiation (kJ/m^2)	G_{IIC} propagation (kJ/m^2)
Warp knitted	0.97 ($\pm$0.05)	2.55 ($\pm$0.16)
Woven	1.32 ($\pm$0.12)	2.80 ($\pm$0.13)
Woven, annealed	1.31 ($\pm$0.09)	2.80 ($\pm$0.26)

Table 5. Experimentally determined mixed mode fracture toughness values (I:II) for the different laminates and loading modes. The 90% confidence limit is given in brackets.

Material	$G_{4:1C}$ initiation (kJ/m^2)	$G_{4:1C}$ propagation (kJ/m^2)	$G_{1:1C}$ initiation (kJ/m^2)	$G_{1:1C}$ propagation (kJ/m^2)	$G_{1:4C}$ initiation (kJ/m^2)	$G_{1:4C}$ propagation (kJ/m^2)
Warp knitted	1.28 (±0.09)	1.79 (±0.15)	1.04 (±0.12)	1.69 (±0.09)	1.39 (±0.17)	2.62 (±0.17)
Woven	1.01 (±0.20)	1.42 (±0.13)	1.20 (±0.20)	1.96 (±0.14)	1.11 (±0.20)	2.23 (-)
Woven, annealed	1.11 (±0.13)	1.89 (±0.40)	0.94 (±0.14)	1.91 (±0.01)	1.03 (±.21)	1.91 (-)

FIGURE CAPTIONS

Figure 1. The three different crack propagation modes [1].

Figure 2. The woven (left) and warp knitted (right) fabrics used for the laminate manufacturing. The warp direction (i.e., 0°) is from left to right in the photographs.

Figure 3. The MMB jig used for Mode II and mixed mode characterization.

Figure 4. An optical micrograph of a polished cross-section in a woven laminate. Matrix pockets (e.g. in the lower right corner) and the crimp in the woven fiber architecture (i.e. the curvature in the fiber bundles running from left to right) are clearly seen. Magnification ×50.

Figure 5. Very clean fibers were seen on most fracture surfaces indicating a poor adhesion between the glass fibers and the PET matrix. The micrograph is taken from a warp knitted mixed mode I:II = 4:1 fracture sample. The global crack propagation direction is from the bottom to the top. Tilt angle 30°.

Figure 6. A typical load/displacement curve from a Mode I test of a warp knitted laminate.

Figure 7. Extensive fiber pull-out seen in a DCB-test behind the crack tip.

Figure 8. Extensive fiber pull-out at the end of the non-adhesive insert of a warp knitted Mode I fracture sample. The variation in fiber angles can be seen. The global crack propagation direction is from the bottom to the top. Tilt angle 10°.

Figure 9. The matrix failure in Mode I took place in a brittle manner. The micrograph shows a fractured matrix pocket and fiber imprints. The global crack propagation direction is from the bottom to the top. Tilt angle 10°.

Figure 10. The general surface appearance of a woven Mode I fracture. The global crack propagation direction is from the bottom to the top. Tilt angle 30°.

Figure 11. A typical load/displacement curve for a woven laminate tested in Mode II.

Figure 12. The typical appearance of a Mode II fracture surface in a woven laminate. Rows of cusps and deformed matrix are seen. The global crack propagation direction is from the bottom to the top. Tilt angle 0°.

Figure 13. Close-up view of cusps on a typical Mode II fracture surface. The global crack propagation direction is from the bottom to the top. Tilt angle 30°.

Figure 14. Many cusps are evident on a Mode II fracture surface of a woven laminate. The global crack propagation direction is from the bottom to the top. Tilt angle 30°.

Figure 15. *Shear deformation of the matrix in a Mode II sample from a warp knitted laminate. The global crack propagation direction is from the bottom to the top. Tilt angle 30°.*

Figure 16. *A large fractured matrix pocket just ahead of the insert in a warp knitted Mode II sample. The global crack propagation direction is from the bottom to the top. Tilt angle 40°.*

Figure 17. *The change of fracture from Mode II (bottom) to Mode I (top) in a warp knitted sample. The surface is smoother and matrix dominated in the Mode II region and rougher with more fiber pull-out in the Mode I region. The global crack propagation direction is from the bottom to the top. Tilt angle 40°.*

Figure 18. *The area around the non-adhesive insert in a woven mixed mode I:II = 4:1 fracture sample at low magnification. The global crack propagation direction is from the bottom to the top. Tilt angle 0°.*

Figure 19. *A large matrix pocket in a woven laminate from a mixed mode I:II = 1:1 fracture surface. The global crack propagation direction is from the bottom to the top. Tilt angle 30°.*

Figure 20. *Misalignment of the glass fibers occurred in the laminates due to, for example, the large flexibility of the commingled fabrics. The micrograph shows the end of an insert in a woven mixed mode I:II = 1:1 sample. The global crack propagation direction is from the bottom to the top. Tilt angle 0°.*

Figure 21. *Cusp like features on the surface of a mixed mode I:II = 1:4 woven sample. The global crack propagation direction is from the bottom to the top. Tilt angle 30°.*

Figure 22. *Cusps at a high magnification from a mixed mode I:II = 1:4 fracture in a woven laminate. The global crack propagation direction is from the bottom to the top. Tilt angle 30°.*

Figure 23. *The formation of cusps at high magnification in a mixed mode I:II = 1:1 warp knitted sample. The global crack propagation direction is from the bottom to the top. Tilt angle 50°.*

Figure 24. *Initiation and propagation fracture toughness data as measured experimentally and predicted analytically using Eq. (1) [8] for the annealed woven material (a), the woven material (b) and the warp knitted material (c).*

Figure 25. *Experimental fracture toughness data and the predicted failure loci for the woven annealed material using a modified form of Charalambides' [8] criterion based on the experimentally assumed cusp angles [7] (compare against Fig. 24a).*
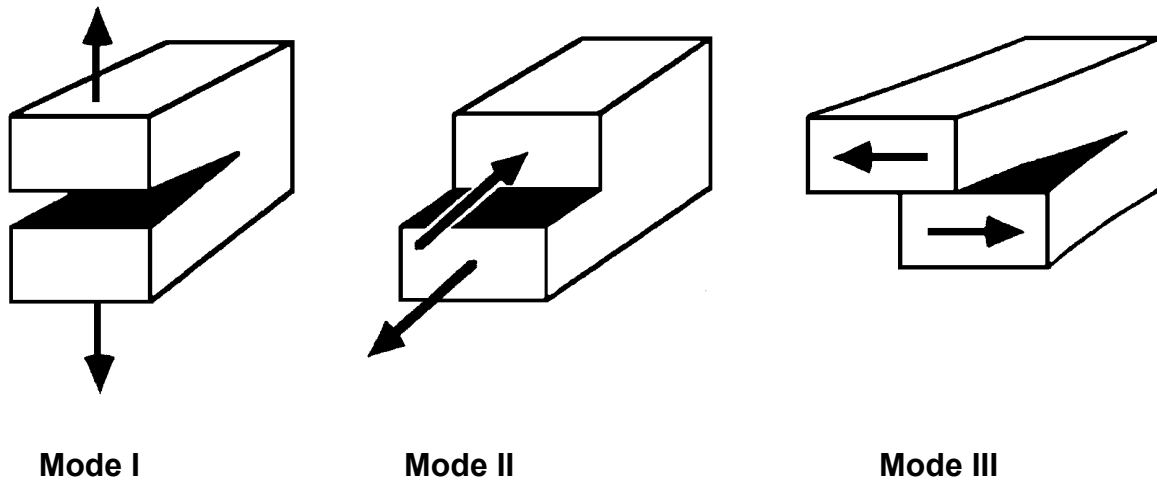
FIGURES

| Mode I | Mode II | Mode III |

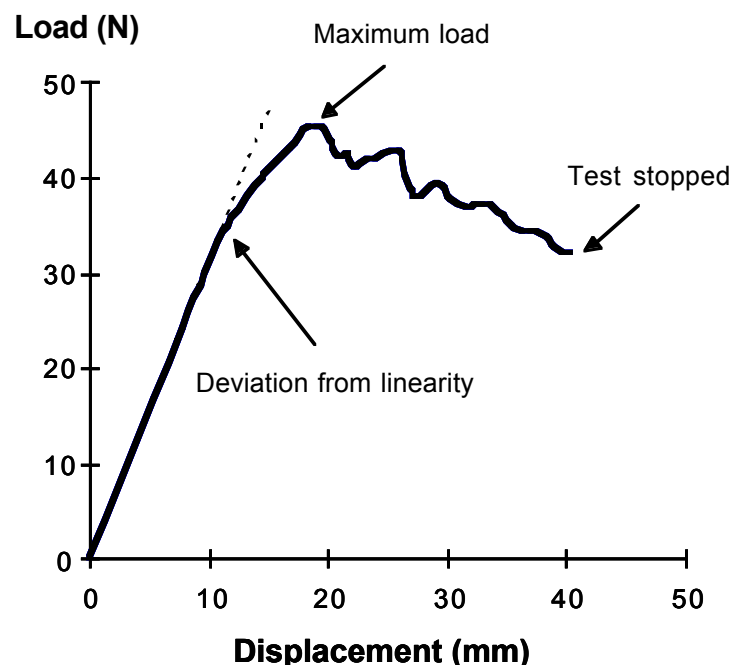**Figure 1.** *The three different crack propagation modes [1].*

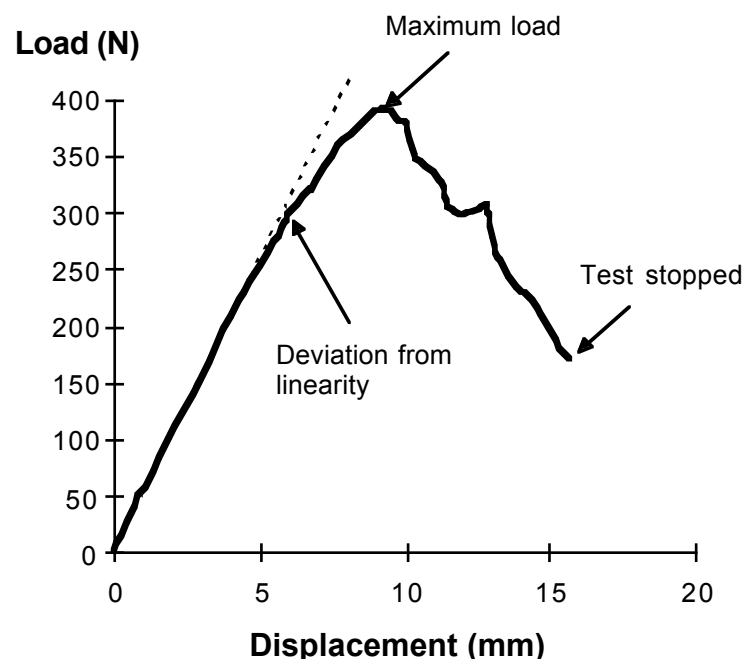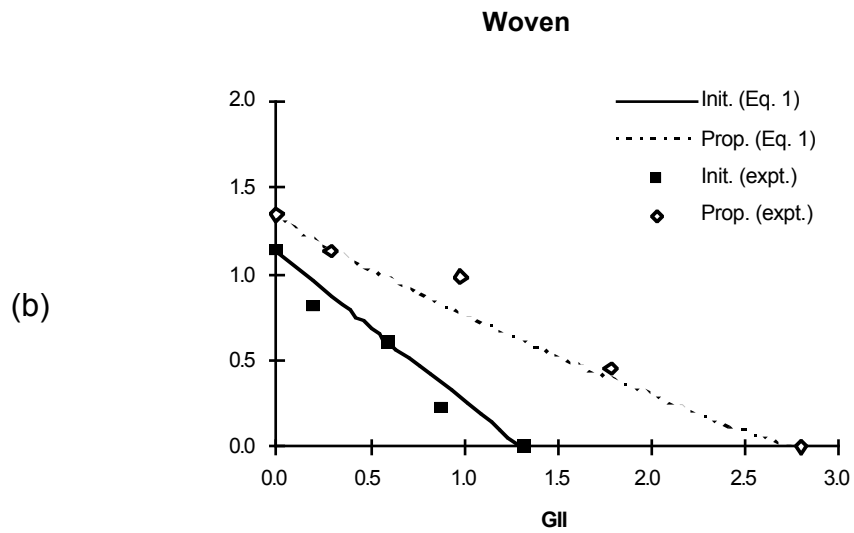*Figure 6. A typical load/displacement curve from a Mode I test of a warp knitted laminate.*
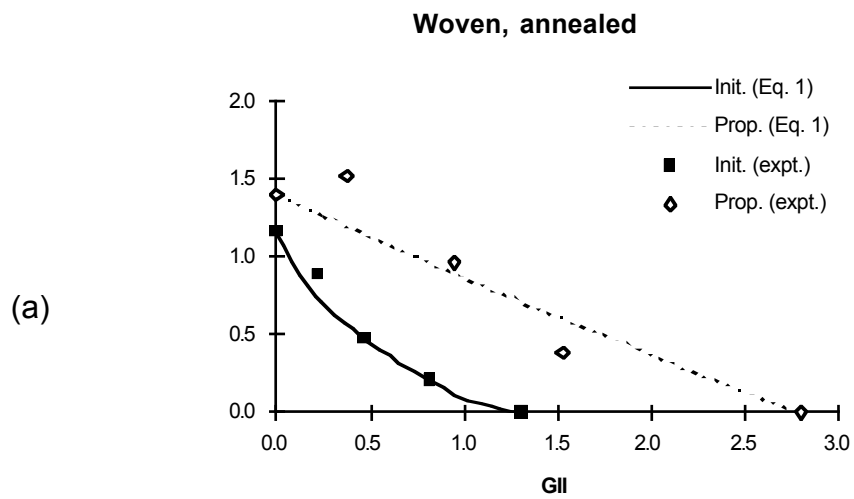
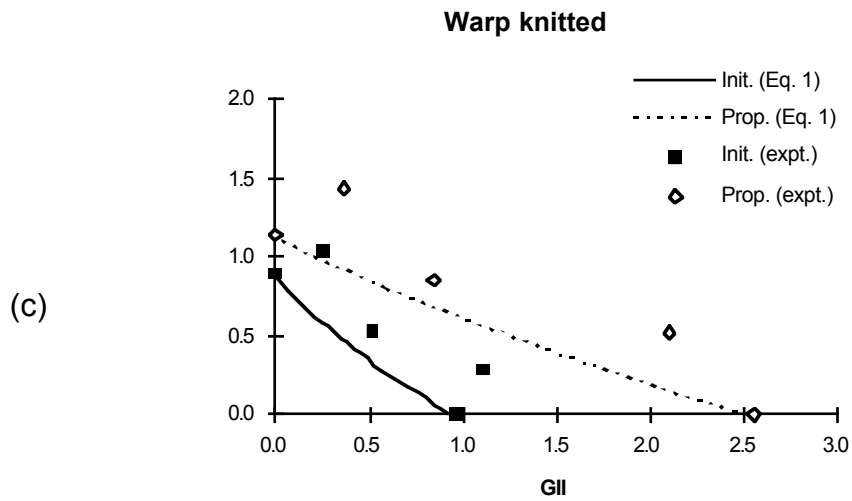*Figure 11. A typical load/displacement curve for a woven laminate tested in Mode II.*

Woven, annealed

(a)

Woven

(b)

Warp knitted

(c)

Figure 24. *Initiation and propagation fracture toughness data as measured experimentally and predicted analytically using Eq. (1) [8] for the annealed woven material (a), the woven material (b) and the warp knitted material (c).*
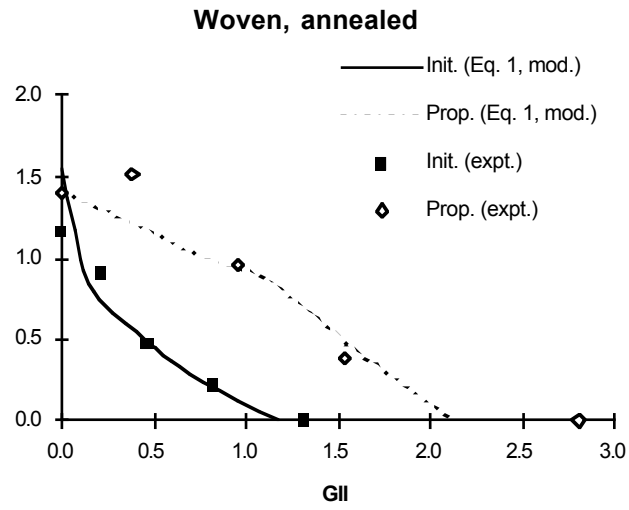
Woven, annealed

Figure 25. Experimental fracture toughness data and the predicted failure loci for the woven annealed material using a modified form of Charalambides' [8] criterion based on the experimentally assumed cusp angles [7] (compared against Fig. 24a).